



JID Open

Selective Depletion of *Staphylococcus aureus* Restores the Skin Microbiome and Accelerates Tissue Repair after Injury

Holly N. Wilkinson^{1,2}, Amber R. Stafford¹, Michelle Rudden^{1,2}, Nina D.C. Rocha¹, Alexandria S. Kidd¹, Sammi Iveson¹, Andrea L. Bell³, Jeffrey Hart³, Ana Duarte⁴, Johan Frieling⁴, Ferd Janssen⁴, Christian Röhrig⁴, Bob de Rooij⁴, Peter F. Ekhart⁵ and Matthew J. Hardman^{1,2}

Our skin is home to a diverse community of commensal microorganisms integral to cutaneous function. However, microbial dysbiosis and barrier perturbation increase the risk of local and systemic infection. *Staphylococcus aureus* is a particularly problematic bacterial pathogen, with high levels of antimicrobial resistance and direct association with poor healing outcome. Innovative approaches are needed to selectively kill skin pathogens, such as *S aureus*, without harming the resident microbiota. In this study, we provide important data on the selectivity and efficacy of an *S aureus*-targeted endolysin (XZ.700) within the complex living skin/wound microbiome. Initial cross-species comparison using Nanopore long-read sequencing identified the translational potential of porcine rather than murine skin for human-relevant microbiome studies. We therefore performed an interventional study in pigs to assess the impact of endolysin administration on the microbiome. XZ.700 selectively inhibited endogenous porcine *S aureus* in vivo, restoring microbial diversity and promoting multiple aspects of wound repair. Subsequent mechanistic studies confirmed the importance of this microbiome modulation for effective healing in human skin. Taken together, these findings strongly support further development of *S aureus*-targeted endolysins for future clinical management of skin and wound infections.

Keywords: Endolysin, Infection, Microbiome, Skin, Wound healing

Journal of Investigative Dermatology (2024) **144**, 1865–1876; doi:10.1016/j.jid.2024.01.018

INTRODUCTION

Our skin is home to a diverse community of predominantly symbiotic microorganisms, collectively known as the microbiota (Byrd et al, 2018). This complex community of microorganisms is integral to skin function, playing wide-ranging roles that span from protection from invading pathogens (Nakatsuji et al, 2017; Zipperer et al, 2016) to suppressing skin tumor development (Nakatsuji et al, 2018). As the largest and most superficial organ of the body, the skin serves as a physical barrier to prevent pathogenic colonization. Nevertheless, breaches to the skin can cause microbial dysbiosis, resulting in skin disease and/or chronic wound infection (Archer et al, 2019; Ganju et al, 2016).

Although the causes of delayed healing are multifactorial (Wilkinson and Hardman, 2020), it is well-established that

colonization by opportunistic pathogens and induction of an inappropriate inflammatory response are key to defective healing (Fazli et al, 2011; Scalise et al, 2015). *Staphylococcus aureus* is one such endemic opportunist and a leading cause of skin and wound infections, persistently and asymptotically colonizing 28–32% of the United States population (Gorwitz et al, 2008). We have previously shown that the bacterial composition of a chronic wound is a clear predictor of whether it will heal (Williams et al, 2018). Moreover, community abundance of *S aureus* is strongly linked to chronic wound healing profile, with specific *S aureus* substrains directly associated with healing outcomes (Kalan et al, 2019). Wounds infected with *S aureus* pose a high risk for patients because they are the most common source of *S aureus*-related bacteremia (Kwiecinski and Horswill, 2020) and the second most common cause of antimicrobial resistance (AMR)-related mortality (Murray et al, 2022).

Unfortunately, front-line antibiotics are largely ineffective at treating wound infections owing to the global prevalence of AMR and the presence of wound bacterial biofilms, aggregate structures that confer AMR by encapsulating bacteria in a protective extracellular polymeric matrix (Wilkinson et al, 2018). AMR *S aureus* strains such as methicillin-resistant *S aureus* (MRSA) are widespread, whereas *S aureus* readily forms biofilms in the wound environment (Guo et al, 2020; James et al, 2008). Serious biofilm infections are frequently treated with combinatorial therapies as standard of care, posing a particularly high risk of toxicity

¹Biomedical Institute for Multimorbidity, Centre for Biomedicine, Hull York Medical School, The University of Hull, Hull, United Kingdom; ²Skin Research Centre, Hull York Medical School, The University of York, Heslington, United Kingdom; ³Cica Biomedical, Knaresborough, United Kingdom; ⁴Microos Pharma B.V., Bilthoven, The Netherlands; and ⁵InnoPact B.V., Ouderkerk aan de Amstel, The Netherlands

Correspondence: Holly N. Wilkinson, Biomedical Institute for Multimorbidity, Centre for Biomedicine, Hull York Medical School, The University of Hull, Daisy Building (2nd Floor), Castle Hill Hospital, Hull HU16 5JQ, United Kingdom. E-mail: h.n.wilkinson@hull.ac.uk

Abbreviations: AMR, antimicrobial resistance; CoNS, coagulase-negative Staphylococci; MRSA, methicillin-resistant *Staphylococcus aureus*

Received 10 November 2023; revised 2 January 2024; accepted 16 January 2024; accepted manuscript published online 1 February 2024; corrected proof published online 19 February 2024

in elderly and immunocompromised patients. Treatment of supposedly susceptible bacteria often fails, whereas some current antibiotics (eg, fluoroquinolones) can increase the risk of MRSA colonization (Tacconelli et al, 2008). Thus, innovative antimicrobial approaches are critically needed to overcome AMR in pathogens, such as *S aureus*, to treat chronic infection while preserving the resident microbiota.

Bacteriophage-derived cell wall-lytic enzymes, known as endolysins, have been suggested as a promising alternative to traditional antibacterial therapies (Röhrig et al, 2020). In contrast to their natural site of action (the inside of the bacterial cell wall), such lysins are capable of degrading the peptidoglycan layer of gram-positive bacteria from the outside, thereby causing cell lysis and death (Haddad Kashani et al, 2017). These endolysins overcome the challenges associated with traditional antibiotics: binding conserved peptidoglycan regions makes resistance development unlikely, whereas endolysins can be targeted to specific bacterial hosts, therefore preventing selective pressure on the resident microbiota (Gondil et al, 2020).

In this study, we determined the specificity and efficacy of a chimeric endolysin, XZ.700, against wound-derived *S aureus* in mixed species biofilms and assessed the subsequent effect of *S aureus* depletion on porcine in vivo and human ex vivo skin repair. The higher taxonomic resolution of long-read sequencing revealed that pigs provide a suitable and relevant model of the human skin microbiome with a high contribution of *Staphylococcus*. We then designed an interventional porcine wound study, demonstrating that XZ.700 maintains potent, targeted efficacy against endogenous *S aureus* within the living skin/wound microbiome. Interestingly, this selective modulation of *S aureus* restored the baseline skin microbiome and accelerated wound repair. Finally, secreted products from an *S aureus*-depleted skin microbiome downregulated inflammation and promoted repair of human skin wounds.

RESULTS

The bacteriophage endolysin XZ.700 selectively inhibits the growth of wound-isolated *S aureus* in single- and mixed-species biofilms

The specificity and efficacy of XZ.700 were first assessed against biofilms of human wound-isolated bacteria. In this study, XZ.700 led to a significant 2–3 log reduction in the growth of methicillin-susceptible *S aureus* ($P < .001$) (Figure 1a) and MRSA ($P < .001$) (Figure 1b) biofilms. By contrast, XZ.700 did not alter the biofilm growth of other *Staphylococci*, such as *S epidermidis* and *S haemolyticus* (Figure 1c) or wound-isolated gram-negative bacteria (*Escherichia coli*, *Klebsiella pneumoniae*, and *Pseudomonas aeruginosa*) (Figure 1d). Live/dead staining of biofilms in situ confirmed XZ.700 effects against MRSA, where treatment significantly reduced viable biofilm thickness ($P < .001$) (Figure 1e and f). Finally, XZ.700 selectivity against MRSA was determined in mixed-species (MRSA: *S epidermidis*) biofilms (Figure 1g–i). In this study, synergistic effects were observed, where XZ.700 showed increased efficacy in mixed-species biofilms, causing a significant 6-log reduction in viable MRSA ($P < .001$) (Figure 1h) with no loss in viable *S epidermidis* (Figure 1i). Together, these data show that XZ.700

exhibits highly selective, potent efficacy against wound-isolated *S aureus* in single- and mixed-species biofilms.

Long-read metagenomic sequencing reveals key similarities in the composition of the porcine and human skin microbiomes, particularly with respect to staphylococcal contribution

In vitro systems are seldom capable of recapitulating the complexity of the living skin microbiome (Larson et al, 2021). Hence, we turned to in vivo model species commonly used in skin research (mouse and pig), comparing their suitability to evaluate staphylococcal modulation of the skin/wound microbiome in a translationally relevant manner. Long-read sequencing revealed high similarity in species richness between human and porcine skin (Figure 2a), whereas mouse skin was significantly less diverse ($P < .01$ – $P < .001$). Genus-level community structure (beta diversity) also revealed significantly greater similarity between pigs and humans than between mice and humans (Figure 2b). Hierarchical clustering further confirmed far higher similarity in bacterial species composition between porcine and human skin, which clustered more closely than between mice and human skin (Figure 2c). Next, relative abundance of the top 10 genera was assessed, where the contribution of *Staphylococcus* was higher in pigs (37%) than in mice (2%) and more closely resembled proportions observed in human skin (54%) (Figure 2d).

A major benefit of long-read metagenomic sequencing is its ability to provide high phylogenetic resolution (Tedersoo et al, 2021), thus enabling the characterization of proportional differences within a single genus (eg, *Staphylococcus*). We thus utilized this technique to assess the contribution of skin *Staphylococci* as a proportion of total bacterial reads, comparing between humans, mice, and pigs (Figure 2e). The human skin microbiome featured the highest overall contribution of different *Staphylococci*. However, porcine skin possessed a greater contribution of most staphylococcal spp than murine skin, with a larger representation of *S aureus*, *S capitis*, *S haemolyticus*, and *S chromogenes* (Figure 2e). These findings demonstrate that human skin displays greater compositional similarity to porcine skin than mouse skin, thus revealing a previously unappreciated aspect of the translational importance of porcine wound studies when considering the preclinical effectiveness of antimicrobial therapies.

XZ.700 selectively inhibits *S aureus* in the porcine skin/wound microbiome

On the basis of our findings demonstrating similarities in skin *Staphylococci* between pigs and humans (Figure 2), we developed a porcine wound model to evaluate the selectivity and efficacy of XZ.700 against *S aureus* in a real-world wound microbiome setting (Supplementary Figure S1). *S aureus* contribution to periwound skin and wounds was determined longitudinally using traditional bacterial culture methods alongside long-read sequencing. Interestingly, vehicle-treated periwound skin and wounds became rapidly colonized by endogenous *S aureus* between day 0 and day 4, which remained elevated throughout the 16-day study (Figure 3a and b). By contrast, XZ.700-treated periwound skin and wounds harbored significantly less viable *S aureus*

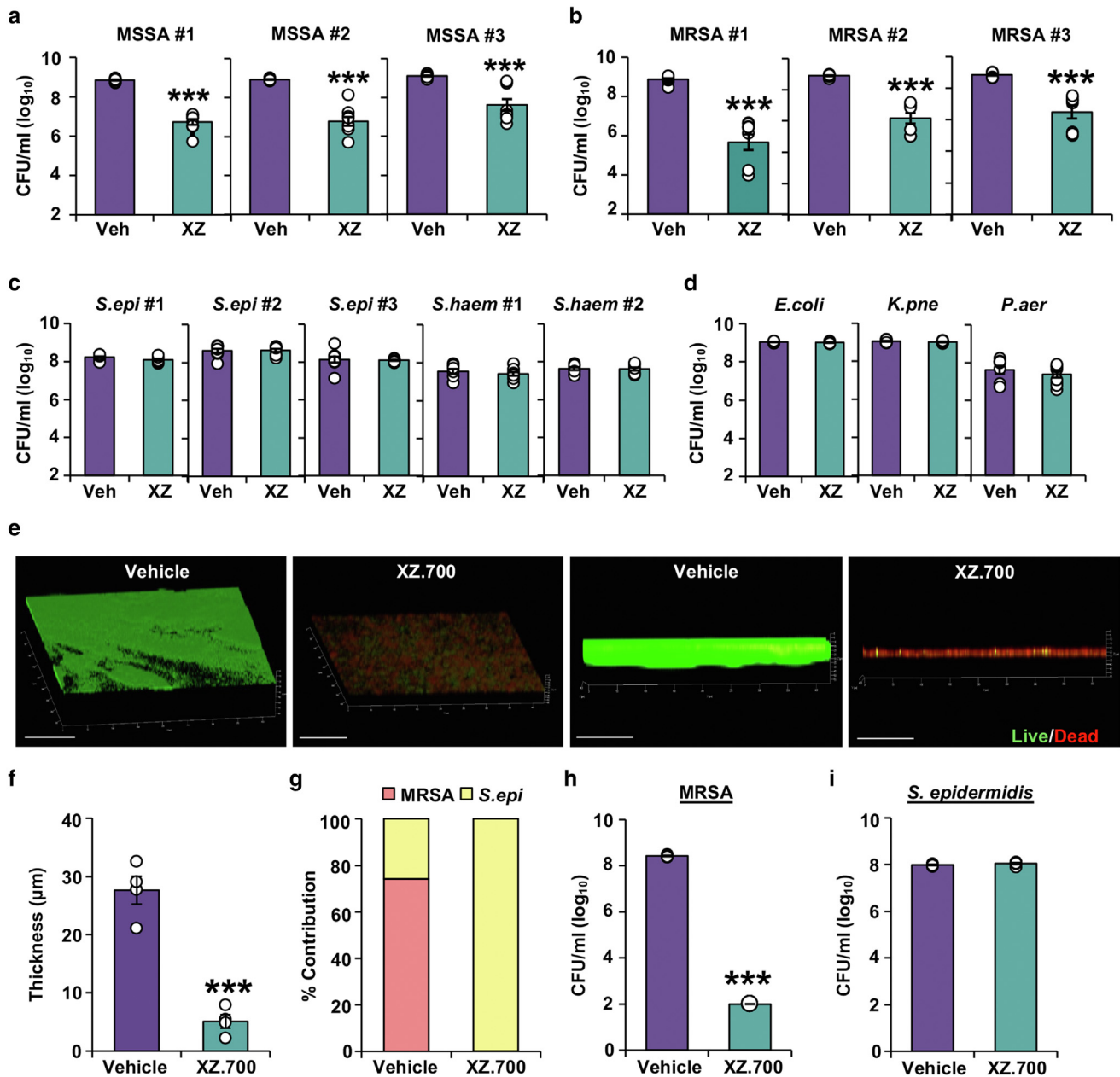


Figure 1. The bacteriophage endolysin, XZ.700, selectively inhibits growth of wound-isolated *S aureus* in single- and mixed-species biofilms. Effect of XZ.700 on membrane biofilms of (a) MSSA; (b) MRSA; (c) *S epidermidis* (denoted as *S. epi*) and *S haemolyticus* (denoted as *S. haem*); and (d) *Escherichia coli* (denoted as *E. coli*), *Klebsiella pneumoniae* (denoted as *K. pne*), and *Pseudomonas aeruginosa* (denoted as *P. aer*). (e) Live:Dead staining of MRSA biofilms with (f) quantification of biofilm thickness. Bar = 100 µm. (g) Percentage contribution of MRSA and *S epidermidis* to mixed-species biofilms with (h, i) absolute counts. Veh = vehicle. XZ = XZ.700 (100 µg/ml). Shown are log₁₀-transformed CFU/ml. Data are presented as mean ± SEM. n = 8–9 biofilms across 3 independent experiments. Independent two-tailed t-tests were performed where ***P < .001. CFU, colony-forming unit; MRSA, methicillin-resistant *Staphylococcus aureus*; MSSA, methicillin-susceptible *Staphylococcus aureus*.

(up to 6 log colony-forming units/cm²; P < .001). Long-read sequencing confirmed reduced *S aureus* presence in XZ.700-treated skin/wounds. In this study, *S aureus* contribution to total staphylococcal reads was significantly lower in XZ.700-treated periwound skin at all time points (P < .01–P < .001) (Figure 3c) and in wounds at days 4 (P < .001) and 12 (P < .05) (Figure 3d).

The proportional distribution of *Staphylococci* was similar in all pretreated skin sites at day 0, with *S aureus* forming approximately 10% of total skin *Staphylococci* (Figure 3e).

By day 4, *S aureus* contribution increased to over 85% of total *Staphylococci* in vehicle-treated regions and remained high throughout the study. By contrast, XZ.700 treated periwound skin and wounds exhibited far lower proportions of *S aureus*. The greatest reduction in *S aureus* was observed on day 12 in periwound skin (over 90% reduction) and day 4 in wounds (over 80% reduction). Interestingly, periwound skin and wounds with *S aureus* depletion showed increased contribution of *S chromogenes*, *S capitis*, and *S haemolyticus*, which more closely mirrored the microbiome profile of

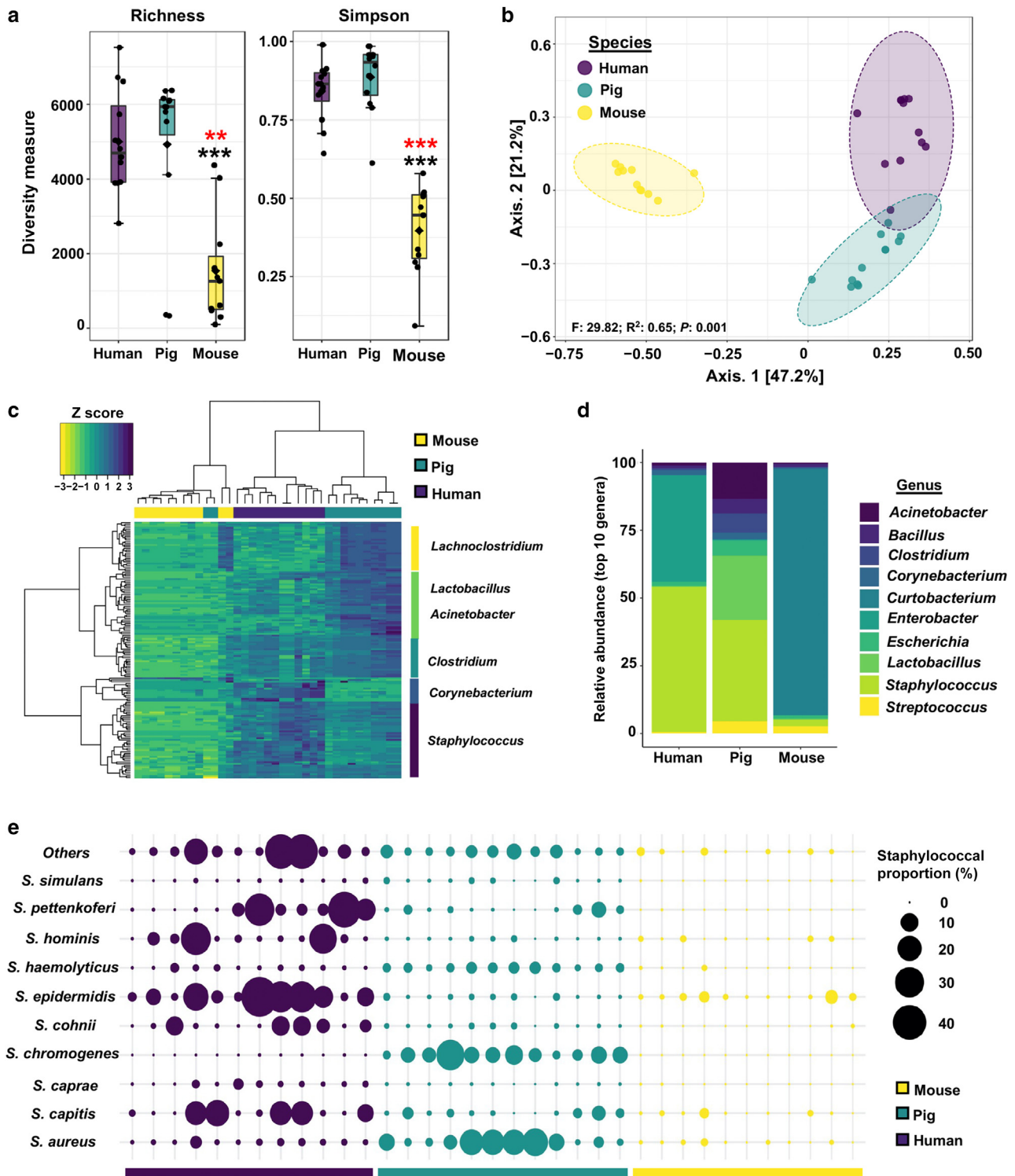


Figure 2. Long-read metagenomic sequencing reveals key similarities in the composition of the porcine and human skin microbiomes, particularly with respect to staphylococcal contribution. (a) Human, porcine, and murine skin swabs (n = 11–12 per group) were taken to assess alpha diversity (richness, Chao; diversity, Simpson). Kruskal–Wallis and Mann–Whitney multiple comparisons were performed, where ***P* < .01 and ****P* < .001. Black asterisks indicate versus human, red asterisks indicate versus pig. (b) Genus-level beta diversity shown through principal coordinate analysis on the basis of Bray–Curtis dissimilarity with PERMANOVA. (c) Hierarchical clustering of the top 150 most variable OTUs with the most featured genus for each cluster. (d) Average relative abundance of top 10 genera and (e) relative abundance of *Staphylococci* for each sample. OTU, operational taxonomic unit; PERMANOVA, permutational ANOVA.

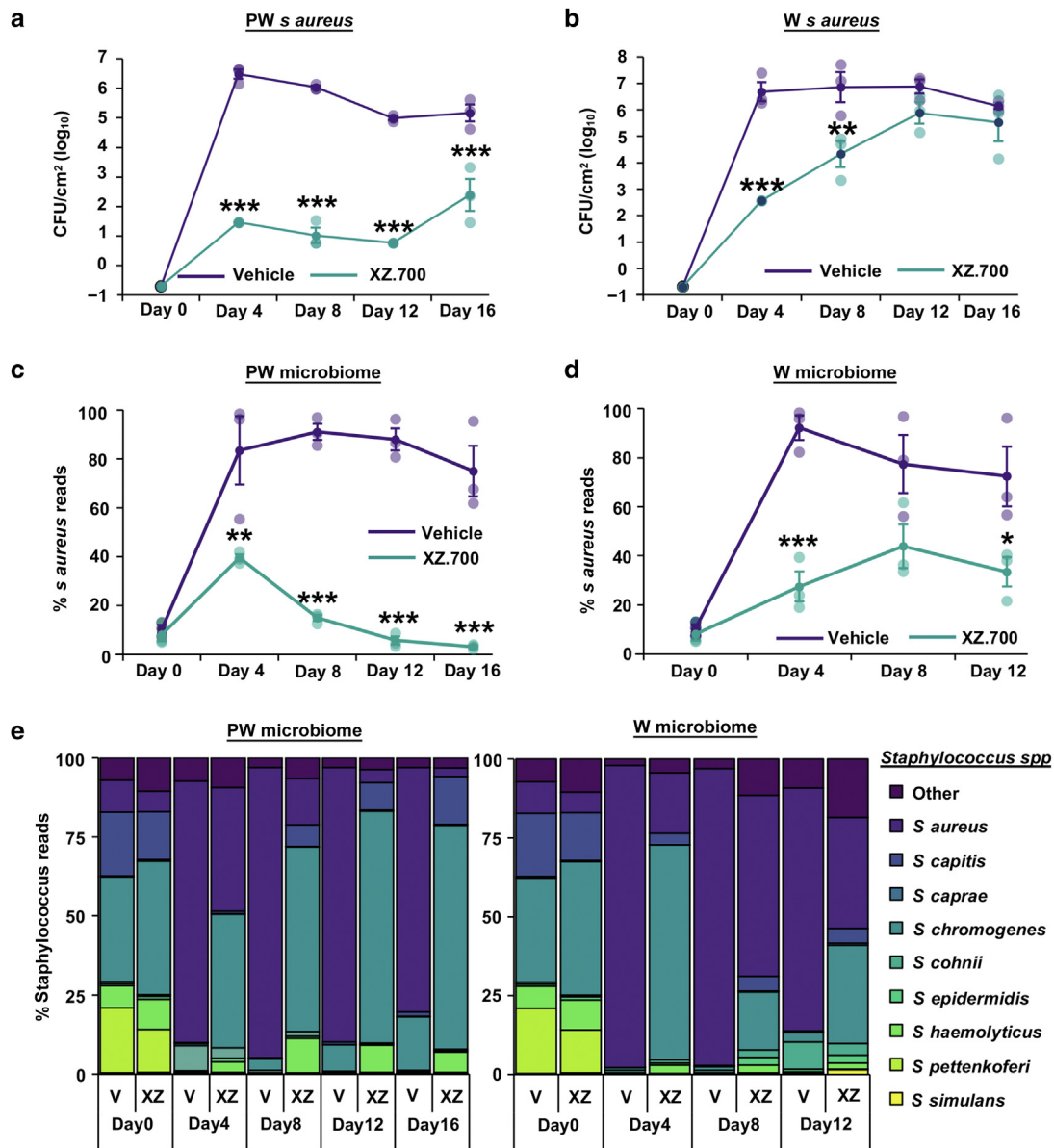


Figure 3. XZ.700 selectively inhibits *S aureus* in the porcine skin/wound microbiome. Direct enumeration of *S aureus* in (a) PW and (b) W swabs. Shown are log₁₀-transformed CFU counts per cm². Metagenomic profiling showing percentage *S aureus* reads relative to total *Staphylococci* for (c) PW and (d) W sites. (e) Average staphylococcal contribution in PW skin and Ws. Veh = vehicle. XZ = XZ.700. Data are presented as mean ± SEM. n = 3 pigs. Two-way ANOVA with Tukey posthoc analysis was performed in a–d where **P* < .05, ***P* < .05, and ****P* < .001. CFU, colony-forming unit; PW, periwound; W, wound.

day 0 skin. Our results reveal that XZ.700 selectively depletes *S aureus* in the periwound skin and wound microenvironment, allowing population with other *Staphylococci* to restore microbial composition to a prewound state.

XZ.700 restores community-level diversity of the porcine skin microbiome after injury-induced colonization by *S aureus*

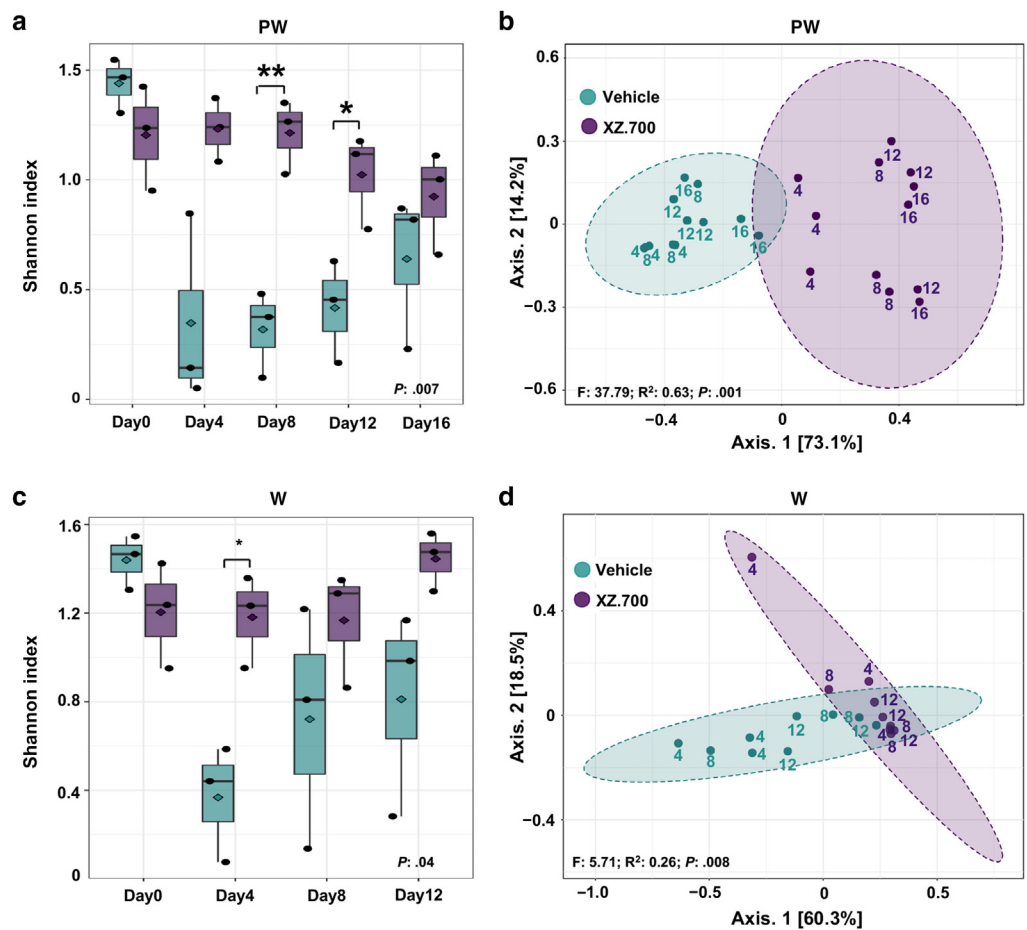
As vehicle-treated porcine wounds became rapidly colonized by *S aureus*, we next explored how modulation of *S aureus* affects microbial community structure. Alpha diversity was greatly reduced in periwound skin (*P* < .01) (Figure 4a) and wounds (*P* < .05) (Figure 4c) after injury, which coincided with increased *S aureus* levels. However, depletion of *S aureus*, using XZ.700, led to significantly higher within

sample diversity at day 4 (wound, *P* < .05), day 8 (periwound, *P* < .01), and day 12 (periwound *P* < .05) after injury. Moreover, species-level beta diversity, visualized using principal coordinate analysis, highlighted distinct clustering of samples based on treatment (vehicle or XZ.700) for periwound skin (*P* = .001) (Figure 4b) and wounds (*P* = .008) (Figure 4d). Consequently, these data highlight that rapid accumulation of *S aureus* after injury is associated with community-level microbial dysbiosis, which is restored by XZ.700 treatment.

Selective depletion of *S aureus* with XZ.700 significantly accelerates porcine skin repair and alters host response

We next determined the effect of XZ.700-related *S aureus* depletion on host wound response (Figure 5). By day 16 after

Figure 4. XZ.700 restores community-level diversity of the porcine skin microbiome after injury-induced colonization by *S aureus*. Swabs were taken from PW and W regions at each assessed time point after injury. n = 3 per group. Alpha diversity for abundant populations is shown by Shannon–Wiener diversity index for (a) PW and (c) W regions. Median estimates were compared between groups using Kruskal–Wallis and Mann–Whitney multiple comparisons. Species-level beta diversity shown through principal coordinate analysis on the basis of Bray–Curtis dissimilarity with PERMANOVA for (b) PW and (d) W regions. PERMANOVA, permutational ANOVA; PW, periwound; W, wound.



injury, most porcine wounds were fully re-epithelialized but with extensive granulation tissue (Figure 5a). Interestingly, XZ.700 treatment significantly reduced wound width ($P < .05$), granulation tissue area ($P < .01$) (Figure 5b), and numbers of infiltrating macrophages in lower ($P < .05$) and upper ($P < .05$) granulation tissue regions (Figure 5c and d). Along with lower overall numbers of macrophages, XZ.700-treated wounds possessed higher percentages of anti-inflammatory arginase-producing macrophages (Figure 5c and e). Moreover, wounds treated with XZ.700 exhibited increased collagen deposition ($P < .05$) (Figure 5f and g) and higher coverage of α -smooth muscle actin staining ($P < .05$) (Figure 5h and i), thus showing increased granulation tissue maturity versus vehicle-treated wounds. Collectively, these findings suggest that selective depletion of *S aureus* promotes multiple aspects of porcine skin repair.

Staphylococcus modulates human skin repair and host response in a species-specific manner

Finally, we extended our findings to determine whether the observed changes in *Staphylococcus* spp across our in vivo porcine study would directly influence human healing. In this study, we isolated several endogenous porcine *Staphylococci* and compared their healing effects with that of human wound—isolated *S aureus* and *S epidermidis* in our established human ex vivo skin model (Wilkinson et al, 2021). Secreted products from porcine and human *S aureus*

significantly delayed healing, whereas other *Staphylococci* did not ($P < .001$) (Figure 6a and b). To increase the translational relevance of our findings, we created mixed communities of porcine *Staphylococci* designed to mimic the levels observed in vehicle- and XZ.700-treated porcine wounds, where the vehicle-modeled group exhibited an *S aureus*-dominated microbiome, and the XZ.700-modeled group exhibited an *S aureus*-depleted microbiome (Figure 6c). Interestingly, we observed that secreted products from the *S aureus*-depleted community (XZ.700 modeled) significantly accelerated human wound closure ($P < .01$) (Figure 6d and e).

RNA-sequencing analysis further demonstrated differential clustering of human wound samples based on microbiome treatment group (Figure 6f). Wounds treated with secreted products from the *S aureus*-depleted (XZ.700-modeled) microbial community showed significant downregulation of key inflammatory genes versus those from the *S aureus*-dominant (vehicle-modeled) group, including *Meiv*, *Oasl*, *Nos2*, *Hla-E*, and *Il17c* (Figure 6g). Functional annotation confirmed these findings, showing that the *S aureus*-dominant (vehicle-modeled) microbiome-induced differentially expressed genes were significantly overrepresented in key Gene Ontology groups and Kyoto Encyclopedia of Genes and Genomes pathways associated with inflammatory processes (Figure 6h). In line with this immune activation activity, we observed a significant decrease in the number of Langerhans

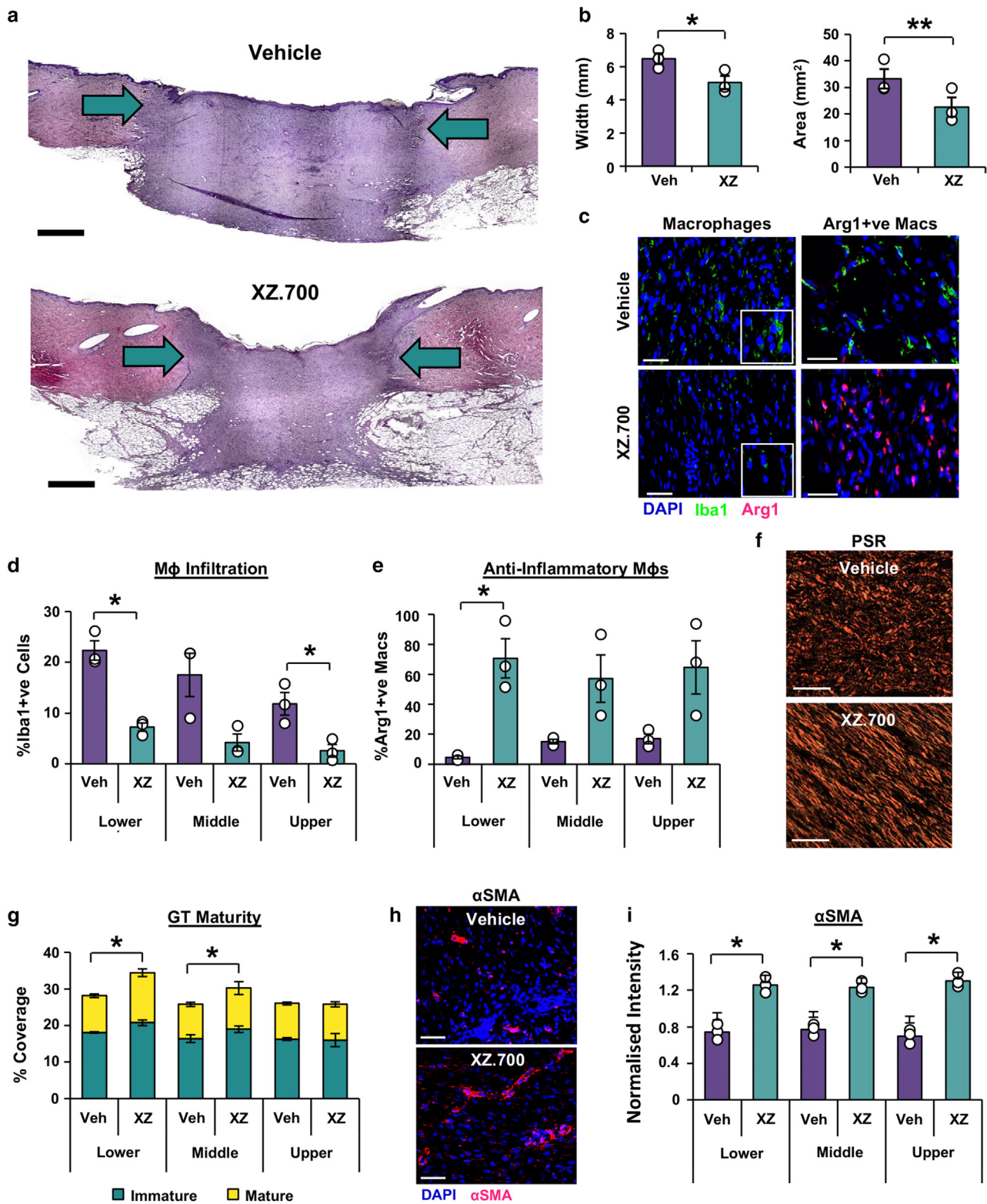


Figure 5. Selective depletion of *S aureus* with XZ.700 significantly accelerates porcine skin repair and alters host response. Representative (a) H&E with quantification of wound width and (b) GT area. Bar = 1 mm. Green arrows = wound margins. (c) Macrophages (%Iba1+ve; Alexa Fluor 488) and arginase-positive macrophages (Alexa Fluor 594) with (d, e) quantification. Bar = 25 μm. DAPI = blue nuclei. Arrows = positive staining. (f) PSR staining and (g) quantification. Bar = 100 μm. α-SMA (h) staining (Alexa Fluor 594) and (i) quantification. Bar = 50 μm. Data are presented as mean ± SEM. n = 3 pigs. Paired *t*-tests were performed, where **P* < .05 and ***P* < .01. α-SMA, α-smooth muscle actin; GT, granulation tissue; PSR, Picrosirius red.

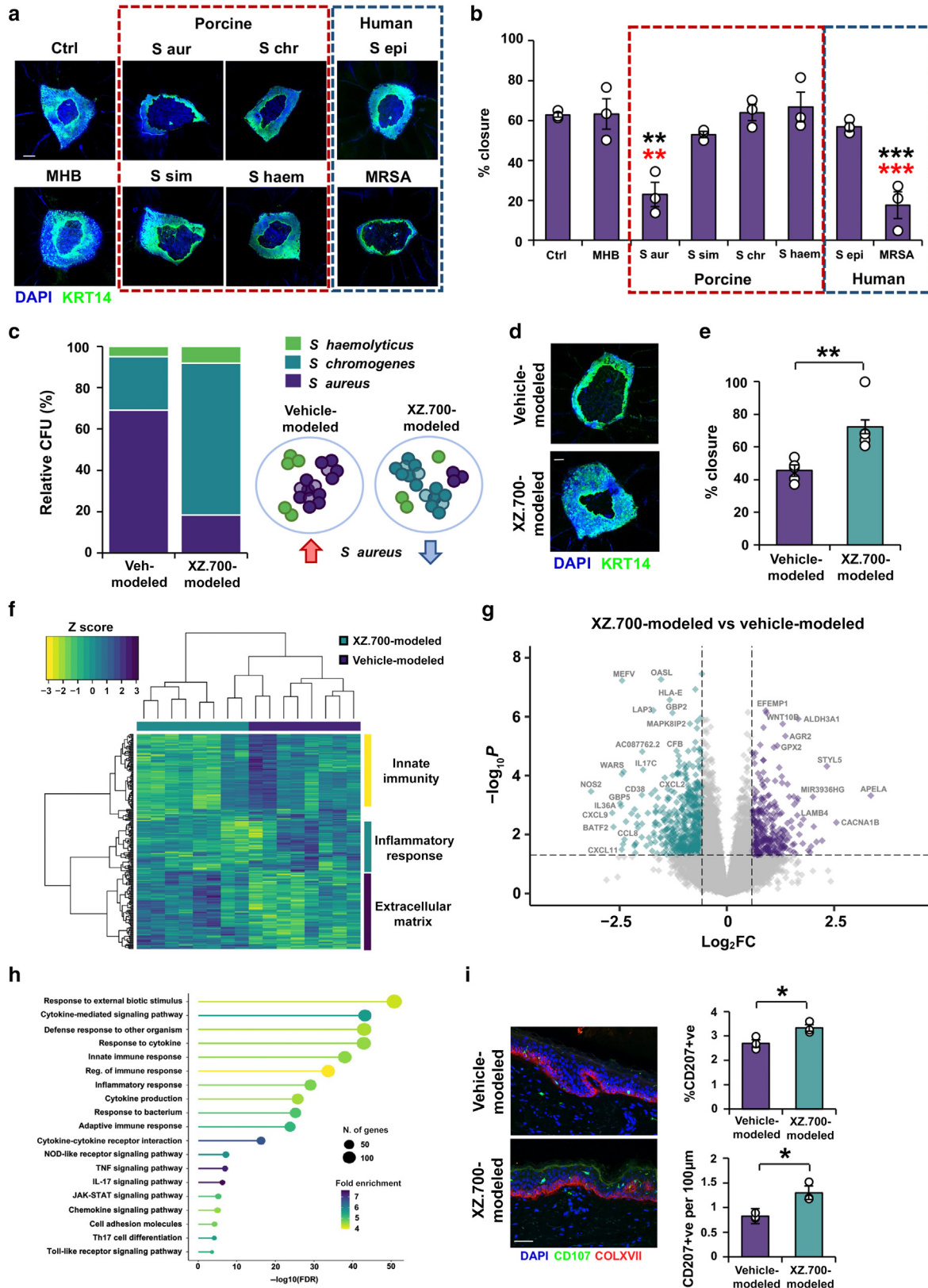


Figure 6. *Staphylococcus* modulates human skin repair and host response in a species-specific manner. (a, b) Secreted products from human and porcine *Staphylococcus* were applied to human ex vivo skin wounds, with wound closure assessed through wholemount staining. Bar = 200 µm. K14 = Alexa Fluor 488. DAPI = nuclei. Secreted products were next isolated from (c) porcine *Staphylococci* grown in mixed communities (relative abundance) with (d, e) corresponding wound closure assessed. RNA sequencing showing (f) hierarchal clustering, (g) volcano plot, and (h) functional annotation comparing differentially expressed genes between vehicle-modeled and XZ.700-modeled groups. (i) Langerin staining of tissue sections (CD207; Alexa Fluor 488) and quantification. Collagen XVII (COLXVII) = Alexa Fluor 594. Bar = 50 µm. Data are presented as mean ± SEM. n = 3 (for b and i), n = 5 (for e), and n = 8 (for f–h). One-way ANOVA with Tukey (b) posthoc and (e, i) independent *t*-tests were performed. **P* < .05, ***P* < .01, and ****P* < .001. K14, keratin 14; MHB, Mueller Hinton Broth.

cells in human skin treated with secreted products from the *S aureus*—dominant (vehicle-modeled) microbiome (Figure 6i), where activated Langerhans migrate from the epidermis to instruct a T-cell effector response (Clayton et al, 2017). These data indicate, to our knowledge, previously unreported potential and importance of selectively targeting skin pathogens for the promotion of human wound healing.

DISCUSSION

Tackling AMR infections will require new antimicrobials that can selectively kill their target pathogen while showing minimal effects on the healthy microbiota of the host (Jang et al, 2020). Targeted antimicrobial therapies are emerging as a promising strategy to tackle AMR infection (Eichenseher et al, 2022; Lu et al, 2021; Röhrig et al, 2020), yet their specificity is seldom assessed in systems harboring a living microbiome, and their subsequent role in modulating host healing responses remains largely uncharacterized. In addition, many studies investigating skin-resident microbial communities utilize short-read sequencing approaches, which retain limited taxonomic resolution (Smythe and Wilkinson, 2023). By contrast, long-read sequencing enables the characterization of bacterial communities beyond species level. This is crucial given that bacteria within a genus and even species can have wide-ranging phenotypes and effects on the host (eg, *Staphylococcus*) (Bosi et al, 2016; Kalan et al, 2019; Krut et al, 2003; Oh et al, 2014). In this study, we identified and implemented a translationally relevant in vivo skin/wound microbiome model, combined with long-read sequencing, to determine the global impact of *S aureus*—targeted modulation on the skin microbiome and subsequent wound repair in vivo.

Our data demonstrate a compositional shift in the skin microbiota of wounded pigs after endolysin treatment, characterized by an increase in alpha diversity. Note, a common observation of human skin pathology is reduced alpha diversity (Gardiner et al, 2017; Zhang et al, 2023). Endolysin-treated skin and wounds exhibited lower *S aureus* levels, with higher proportions of coagulase-negative *Staphylococci* (CoNS), which more closely mirrored the staphylococcal contribution of healthy porcine skin. In our human ex vivo model, secreted products from an *S aureus*—dominant microbiome delayed healing and reduced Langerhans cell numbers. This is in line with an immune activation phenotype, where activated Langerhans cells migrate out of the epidermis to initiate a T-cell effector response (Clayton et al, 2017). By contrast, a CoNS-dominant microbial mix enabled epidermal retention of Langerhans cells and promoted healing in human skin. Interestingly, there is an increase in epidermal retention of Langerhans cells in diabetic foot ulcers that heal within 4 weeks versus in those that do not heal (Stojadinovic et al, 2013), whereas the presence of Langerhans cells is also required for appropriate skin repair in mice (Wasko et al, 2022). Hence, these findings suggest that depletion of *S aureus*—secreted products may accelerate ex vivo skin healing by enabling epidermal retention of Langerhans cells.

Previous studies demonstrate the importance of CoNS in mediating effective repair, such as by inhibiting excessive inflammation (Lai et al, 2009; Li et al, 2019) and accelerating

wound closure (Luqman et al, 2020). Crucially, CoNS, such as *S capitis* and *S epidermidis*, produce antimicrobials that selectively kill *S aureus* and other opportunistic skin pathogens (Cogen et al, 2010; O'Neill et al, 2020; Nakatsuji et al, 2017), and CoNS preapplication can even prevent *S aureus* colonization in the nares of mice and humans (Iwase et al, 2010; Park et al, 2011). *S aureus*—specific antimicrobials may therefore provide enhanced efficacy over broad-spectrum treatments by supporting the beneficial effects of CoNS.

S aureus remains the most prevalent contributor to skin and chronic wound infection (Macdonald et al, 2021; Parlet et al, 2019; Verbanic et al, 2020); thus, therapies targeted against *S aureus* could revolutionize clinical treatment strategies. Endogenous phage lysins (LysGH15 and LysP53) have previously shown efficacy against *S aureus* on murine skin in vivo (Cheng et al, 2018) and porcine skin ex vivo (Li et al, 2022). XZ.700 is a chimeric endolysin combining lysostaphin with components of the *S aureus* bacteriophage endolysin, Ply2638, for high selectivity (Kuiper et al, 2021). Moreover, XZ.700 shows promise in combating AMR because both methicillin-susceptible *Staphylococcus aureus* and MRSA fail to develop resistance to XZ.700 after repeated cycles of exposure (Eichenseher et al, 2022).

We and others have confirmed the selectivity of XZ.700 using in vitro, ex vivo, and murine in vivo models (Eichenseher et al, 2022; Kuiper et al, 2021; Pallesen et al, 2023). Now, we provide, to our knowledge, previously unreported data on the specificity and efficacy of XZ.700 against *S aureus* within a complex living skin/wound microbiome. Indeed, our results reveal that skin and wounds treated with XZ.700 harbor greater microbial diversity than control wounds. This is essential given that chronic non-healing wounds are characterized by reduced microbial diversity (Gardiner et al, 2017; Zhang et al, 2023), whereas broad-spectrum antibiotics further cause microbial dysbiosis (Dellacecca et al, 2020; Jin et al, 2016), delay repair in murine skin wounds (Zhang et al, 2015), and enable AMR strains to populate in some cases (Schwartz et al, 2020).

Porcine skin more closely resembles the anatomical and physiological features of human skin than any other non-primate animal research model (Summerfield et al, 2015). Immunological similarities between human and porcine skin have also been observed, such as identification of porcine dendritic cell subsets that are transcriptionally comparable with those of human (Marquet et al, 2014) and demonstration that porcine macrophages display human-relevant surface markers and similar phenotypic responses to lipopolysaccharide (Ezquerria et al, 2009; Meli et al, 2021). Importantly, we now show that the porcine skin microbiome better recapitulates that of humans (than that of mice does), especially with respect to *Staphylococci* colonization. The key disparities between human and murine microbiomes have been noted previously, even suggesting that mice are poor candidates for the development of *S aureus*—targeted vaccines (Mrochen et al, 2020; Trübe et al, 2019). However, host response to pathogens remains more widely characterized in mice owing to their greater tractability.

Despite the clear advantages of our porcine in vivo studies, a limitation of our approach is focusing solely on female pigs.

It is recognized that males and females differ in their immunological responses (Klein and Flanagan, 2016), with previous studies demonstrating a role for biological sex in clearance of bacterial infection, which appears to be tissue and bacteria specific. For example, male mice cleared *S aureus* from their skin more rapidly than female mice (Eichenseher et al, 2022), whereas in the lung, female mice cleared *P aeruginosa* more effectively than male mice (Pittet et al, 2021). Future investigations should therefore consider the potential sex-specific differences in the microbiome and the subsequent consequences of microbiome modulation on host wound response.

Collectively, our data provide, to our knowledge, previously unreported demonstration of the potent efficacy of a chimeric endolysin for the selective removal of *S aureus* within the living skin/wound microbiome. Our findings are fundamentally important in the context of widespread AMR resulting from inappropriate use of traditional antibiotics. It is now clear that maintenance of the resident microbiota limits pathogenic colonization, yet further work is required to fully elucidate the mechanisms by which commensals protect against infection and mediate effective tissue repair. Nevertheless, targeted antimicrobials offer a promising therapeutic strategy for the future management of skin and wound infections.

MATERIALS AND METHODS

Bacterial culture

Human wound bacterial isolates were obtained from Hull Royal Infirmary, and their classification was confirmed using a Vitek 2 (bioMérieux, Marcy-l'Étoile, France). Bacteria were seeded on polycarbonate membranes and treated with XZ.700 (100 µg/ml) or vehicle (0.01% Tween 20 in distilled water) 2 hours after seeding and collected for enumeration or live/dead staining 16 hours after seeding. Further details are provided in the [Supplementary Materials and Methods](#).

Comparison of porcine, murine, and human microbiome

Normal skin swabs were taken from 12 minipigs (female, aged ~6 months), 11 mice (female, aged 8 weeks, C57Bl/6j; Charles River Laboratories), and 12 humans (aged 61–73 years; 10 female, 2 male) to compare relative microbiota proportions. Skin was swabbed using PBS-saturated FLOQ swabs (Copan Diagnostics, Murrieta, CA), and DNA was isolated using the DNeasy PowerSoil Pro Kit (Qiagen, Hilden, Germany). Library preparation was undertaken using the Rapid PCR Barcoding Kit (SQK-RPB004), and DNA sequencing was performed on a GridION platform (both from Oxford Nanopore Technologies, Oxford, United Kingdom). Details of sequence processing and analysis are provided in the [Supplementary Materials and Methods](#).

Animal experimentation

Three female Gottingen Minipigs (aged ~6 months and weighing ~16 kg) were obtained from Ellegaard Minipigs and housed at the University of Leeds under a 12-hour light:dark cycle with once daily feeding and water provided ad libitum. Animal procedures were carried out under full United Kingdom Home Office regulations (project license P81E9540D). Further details are provided in the [Supplementary Materials and Methods](#).

Histological analysis

Paraffin-embedded sections (6 µm thick) were dewaxed and rehydrated to distilled water before H&E, picosirius red, and immunofluorescence staining. Full details are provided in the [Supplementary Materials and Methods](#).

Human ex vivo wounding

Abdominal human skin was collected from surgical theaters at Castle Hill Hospital under full written, informed patient consent and institutional approval (University of Hull; LREC: 17/SC/0220). Wound healing effects of a subset of porcine and human *Staphylococci* were determined using our established human ex vivo skin wounding model (Wilkinson et al, 2021).

RNA sequencing

RNA was extracted from human ex vivo wounds by homogenizing in TRIzol and purifying using the PureLink RNA Mini Kit (Thermo Fisher Scientific, Waltham, MA). RNA sequencing was performed as described in the [Supplementary Materials and Methods](#).

Statistical analyses

Mean + SEM was used for nonsequencing data. Independent 2-tailed student's *t*-tests compared between vehicle and XZ.700 in biofilm culture experiments. Alpha diversity median estimates were compared between groups using Kruskal–Wallis with Mann–Whitney multiple comparisons tests. Permutational ANOVA determined significant differences in beta diversity between groups. Two-way ANOVA with Tukey posthoc enabled comparison of XZ.700 efficacy with *S aureus* peri-wound/wound abundance. Pairwise *t*-tests were performed on datasets comparing minipig healing (vehicle vs XZ.700). Independent two-tailed student's *t*-tests and one-way ANOVA with Tukey posthoc were used to assess host response to bacterial supernatants. Data were deemed significant where $P < .05$.

DATA AVAILABILITY STATEMENT

The data that support the findings of this study are available from the corresponding author upon reasonable request. Datasets related to this article can be found at <https://www.ncbi.nlm.nih.gov/bioproject/PRJNA1031137> and <https://www.ncbi.nlm.nih.gov/bioproject/PRJNA1032892>, hosted at the Sequence Read Archive database under accession numbers PRJNA1031137 and PRJNA1032892.

ORCIDs

Holly N. Wilkinson: <http://orcid.org/0000-0002-8453-7264>
 Amber R. Stafford: <http://orcid.org/0000-0002-2684-2826>
 Michelle Rudden: <http://orcid.org/0000-0001-9617-087X>
 Nina D.C. Rocha: <http://orcid.org/0000-0002-6941-9876>
 Alexandria S. Kidd: <http://orcid.org/0009-0003-2487-5792>
 Sammi Iveson: <http://orcid.org/0000-0003-4501-9437>
 Andrea L. Bell: <http://orcid.org/0009-0004-7890-0882>
 Jeffrey Hart: <http://orcid.org/0000-0001-6917-3637>
 Ana Duarte: <http://orcid.org/0009-0002-0537-1700>
 Johan Frieling: <http://orcid.org/0000-0002-0569-1221>
 Ferd Janssen: <http://orcid.org/0000-0003-3144-3376>
 Christian Röhrig: <http://orcid.org/0000-0003-4647-1011>
 Bob de Rooij: <http://orcid.org/0000-0002-6424-0025>
 Peter F. Ekhardt: <http://orcid.org/0000-0002-0164-2633>
 Matthew J. Hardman: <http://orcid.org/0000-0002-6423-5074>

CONFLICT OF INTEREST

FJ was an employee of Microcos Pharma until January 2023. CR, PFE, and BD are current employees of Microcos Pharma B.V. PFE has shares in Microcos Pharma B.V through Innopact B.V. A patent exists for the invention and medical use of XZ.700 (international publication number WO, 2017/046021). The remaining authors state no conflict of interest.

ACKNOWLEDGMENTS

This work was supported by Microcos Pharma B.V., in collaboration with the University of Hull and Cica Biomedical, along with funding to HNW from the

National Biofilms Innovation Centre (04POC21-228 and BB/S508020/NBIC_FTMA3_21_007). We would specifically like to thank the Daisy Appeal for providing laboratory facilities, the support of the University of Leeds and University of Hull Biological Services Units, and Paolo Matteucci and the surgical team for providing access to human skin.

AUTHOR CONTRIBUTIONS

Conceptualization: HNW, JH, JF, CR, BD, PFE, MJH; Data Curation: HNW, ARS, MR, NDCR, ASK, SI, ALB, JH; Formal Analysis: HNW, ARS, MR; Funding Acquisition: HNW; Investigation: HNW, ARS, NDCR, ASK, SI, ALB, JH; Methodology: HNW, JH, MJH; Project Administration: HNW, JH, ALB, JF, BdR, PFE, MJH; Resources: HNW, JH, AD, JF, CR, BdR, PFE, MJH; Software: HNW, ARS, MR; Supervision: HNW, JH, BdR, PFE, MJH; Validation: HNW, ARS, MR, NDCR, ASK, SI, ALB, JH; Visualization: HNW, ARS, MR; Writing – Original Draft Preparation: HNW; Writing – Review and Editing: HNW, JH, JF, CR, BdR, PFE, MJH

SUPPLEMENTARY MATERIAL

Supplementary material is linked to the online version of the paper at www.jidonline.org, and at <https://doi.org/10.1016/j.jid.2024.01.018>.

REFERENCES

- Archer NK, Jo JH, Lee SK, Kim D, Smith B, Ortines RV, et al. Injury, dysbiosis, and filaggrin deficiency drive skin inflammation through keratinocyte IL-1 α release. *J Allergy Clin Immunol* 2019;143:1426–43.e6.
- Bosi E, Monk JM, Aziz RK, Fondi M, Nizet V, Palsson BØ. Comparative genome-scale modelling of *Staphylococcus aureus* strains identifies strain-specific metabolic capabilities linked to pathogenicity. *Proc Natl Acad Sci USA* 2016;113:E3801–9.
- Byrd AL, Belkaid Y, Segre JA. The human skin microbiome. *Nat Rev Microbiol* 2018;16:143–55.
- Cheng M, Zhang L, Zhang H, Li X, Wang Y, Xia F, et al. An ointment consisting of the phage lysin LysGH15 and apigenin for decolonization of methicillin-resistant *Staphylococcus aureus* from skin wounds. *Viruses* 2018;10:244.
- Clayton K, Vallejo AF, Davies J, Sirvent S, Polak ME. Langerhans cells—programmed by the epidermis. *Front Immunol* 2017;8:1676.
- Cogen AL, Yamasaki K, Muto J, Sanchez KM, Crotty Alexander LC, Tanios J, et al. *Staphylococcus epidermidis* antimicrobial δ -toxin (phenol-soluble modulins- γ) cooperates with host antimicrobial peptides to kill group A *Streptococcus*. *PLoS One* 2010;5:e8557.
- Dellacecca ER, Cosgrove C, Mukhatayev Z, Akhtar S, Engelhard VH, Rademaker AW, et al. Antibiotics drive microbial imbalance and vitiligo development in mice. *J Invest Dermatol* 2020;140:676–87.e6.
- Eichenseher F, Herpers BL, Badoux P, Leyva-Castillo JM, Geha RS, van der Zwart M, et al. Linker-improved chimeric endolysin selectively kills *Staphylococcus aureus* in vitro, on reconstituted human epidermis, and in a murine model of skin infection. *Antimicrob Agents Chemother* 2022;66:e0227321.
- Ezquerria A, Revilla C, Alvarez B, Pérez C, Alonso F, Domínguez J. Porcine myelomonocytic markers and cell populations. *Dev Comp Immunol* 2009;33:284–98.
- Fazli M, Bjarnsholt T, Kirketerp-Møller K, Jørgensen A, Andersen CB, Givskov M, et al. Quantitative analysis of the cellular inflammatory response against biofilm bacteria in chronic wounds. *Wound Repair Regen* 2011;19:387–91.
- Ganju P, Nagpal S, Mohammed MH, Nishal Kumar P, Pandey R, Natarajan VT, et al. Microbial community profiling shows dysbiosis in the lesional skin of vitiligo subjects. *Sci Rep* 2016;6:18761.
- Gardiner M, Vicaretti M, Sparks J, Bansal S, Bush S, Liu M, et al. A longitudinal study of the diabetic skin and wound microbiome. *PeerJ* 2017;5:e3543.
- Gondil VS, Harjai K, Chhibber S. Endolysins as emerging alternative therapeutic agents to counter drug-resistant infections. *Int J Antimicrob Agents* 2020;55:105844.
- Gorwitz RJ, Kruszon-Moran D, McAllister SK, McQuillan G, McDougal LK, Fosheim GE, et al. Changes in the prevalence of nasal colonization with *Staphylococcus aureus* in the United States, 2001–2004. *J Infect Dis* 2008;197:1226–34.
- Guo Y, Song G, Sun M, Wang J, Wang Y. Prevalence and therapies of antibiotic-resistance in *Staphylococcus aureus*. *Front Cell Infect Microbiol* 2020;10:107.
- Haddad Kashani H, Schmelcher M, Sabzalipoor H, Seyed Hosseini E, Moniri R. Recombinant endolysins as potential therapeutics against antibiotic-resistant *Staphylococcus aureus*: current status of research and novel delivery strategies. *Clin Microbiol Rev* 2017;31:e00071–17.
- Iwase T, Uehara Y, Shinji H, Tajima A, Seo H, Takada K, et al. *Staphylococcus epidermidis* Esp inhibits *Staphylococcus aureus* biofilm formation and nasal colonization. *Nature* 2010;465:346–9.
- James GA, Swogger E, Wolcott R, Pulcini ED, Secor P, Sestrich J, et al. Biofilms in chronic wounds. *Wound Repair Regen* 2008;16:37–44.
- Jang IT, Yang M, Kim HJ, Park JK. Novel cytoplasmic bacteriocin compounds derived from *Staphylococcus epidermidis* selectively kill *Staphylococcus aureus*, including methicillin-resistant *Staphylococcus aureus* (MRSA). *Pathogens* 2020;9:87.
- Jin Y, Wu Y, Zeng Z, Jin C, Wu S, Wang Y, et al. From the cover: exposure to oral antibiotics induces gut microbiota dysbiosis associated with lipid metabolism dysfunction and low-grade inflammation in mice. *Toxicol Sci* 2016;154:140–52.
- Kalan LR, Meisel JS, Loesche MA, Horwinski J, Soaita I, Chen X, et al. Strain- and species-level variation in the microbiome of diabetic wounds is associated with clinical outcomes and therapeutic efficacy. *Cell Host Microbe* 2019;25:641–55.e5.
- Klein SL, Flanagan KL. Sex differences in immune responses. *Nat Rev Immunol* 2016;16:626–38.
- Krut O, Utermöhlen O, Schlossherr X, Krönke M. Strain-specific association of cytotoxic activity and virulence of clinical *Staphylococcus aureus* isolates. *Infect Immun* 2003;71:2716–23.
- Kuiper JWP, Hogervorst JMA, Herpers BL, Bakker AD, Klein-Nulend J, Nolte PA, et al. The novel endolysin XZ.700 effectively treats MRSA biofilms in two biofilm models without showing toxicity on human bone cells in vitro. *Biofouling* 2021;37:184–93.
- Kwiecek JM, Horswill AR. *Staphylococcus aureus* bloodstream infections: pathogenesis and regulatory mechanisms. *Curr Opin Microbiol* 2020;53:51–60.
- Lai Y, Di Nardo A, Nakatsuji T, Leichte A, Yang Y, Cogen AL, et al. Commensal bacteria regulate toll-like receptor 3–dependent inflammation after skin injury. *Nat Med* 2009;15:1377–82.
- Larson PJ, Chong D, Fleming E, Oh J. Challenges in developing a human model system for skin microbiome research. *J Invest Dermatol* 2021;141:228–31.e4.
- Li C, Nyaruaba R, Zhao X, Xue H, Li Y, Yang H, et al. Thermosensitive hydrogel wound dressing loaded with bacteriophage lysin LysP53. *Viruses* 2022;14:1956.
- Li D, Wang W, Wu Y, Ma X, Zhou W, Lai Y. Lipopeptide 78 from *Staphylococcus epidermidis* activates β -catenin to inhibit skin inflammation. *J Immunol* 2019;202:1219–28.
- Lu Y, Wang Y, Wang J, Zhao Y, Zhong Q, Li G, et al. Phage endolysin LysP108 showed promising antibacterial potential against methicillin-resistant *Staphylococcus aureus*. *Front Cell Infect Microbiol* 2021;11:668430.
- Luqman A, Muttaqin MZ, Yulaipi S, Ebner P, Matsuo M, Zabel S, et al. Trace amines produced by skin bacteria accelerate wound healing in mice. *Commun Biol* 2020;3:277.
- Macdonald KE, Boeckh S, Stacey HJ, Jones JD. The microbiology of diabetic foot infections: a meta-analysis. *BMC Infect Dis* 2021;21:770.
- Marquet F, Vu Manh TP, Maisonnasse P, Elhrouzi-Younes J, Urien C, Bouguyon E, et al. Pig skin includes dendritic cell subsets transcriptomically related to human CD1a and CD14 dendritic cells presenting different migrating behaviors and T cell activation capacities. *J Immunol* 2014;193:5883–93.
- Meli VS, Donahue RP, Link JM, Hu JC, Athanasiou KA, Liu WF. Isolation and characterization of porcine macrophages and their inflammatory and fusion responses in different stiffness environments. *Biomater Sci* 2021;9:7851–61.
- Mrochen DM, Fernandes de Oliveira LM, Raafat D, Holtfreter S. *Staphylococcus aureus* host tropism and its implications for murine infection models. *Int J Mol Sci* 2020;21:7061.
- Murray CJ, Ikuta KS, Sharara F, Swetschinski L, Aguilar GR, Gray A. Global burden of bacterial antimicrobial resistance in 2019: a systematic analysis

- [published correction appears in Lancet 2022;400:1102]. Lancet 2022;399:629–55.
- Nakatsuji T, Chen TH, Butcher AM, Trzoss LL, Nam SJ, Shirakawa KT, et al. A commensal strain of *Staphylococcus epidermidis* protects against skin neoplasia. *Sci Adv* 2018;4:eaao4502.
- Nakatsuji T, Chen TH, Narala S, Chun KA, Two AM, Yun T, et al. Antimicrobials from human skin commensal bacteria protect against *Staphylococcus aureus* and are deficient in atopic dermatitis. *Sci Transl Med* 2017;9:eaah4680.
- O'Neill AM, Nakatsuji T, Hayachi A, Williams MR, Mills RH, Gonzalez DJ, et al. Identification of a human skin commensal bacterium that selectively kills *Cutibacterium acnes*. *J Invest Dermatol* 2020;140:1619–28.e2.
- Oh J, Byrd AL, Deming C, Conlan S, NISC Comparative Sequencing Program, Kong HH, et al. Biogeography and individuality shape function in the human skin metagenome. *Nature* 2014;514:59–64.
- Pallesen EMH, Gluud M, Vadivel CK, Buus TB, de Rooij B, Zeng Z, et al. Endolysin inhibits skin colonization by patient-derived *Staphylococcus aureus* and malignant T-cell activation in cutaneous T-cell lymphoma. *J Invest Dermatol* 2023;143:1757–68.e3.
- Park B, Iwase T, Liu GY. Intranasal application of *S. epidermidis* prevents colonization by methicillin-resistant *Staphylococcus aureus* in mice. *PLoS One* 2011;6:e25880.
- Parlet CP, Brown MM, Horswill AR. Commensal staphylococci influence *Staphylococcus aureus* skin colonization and disease. *Trends Microbiol* 2019;27:497–507.
- Pittet JF, Hu PJ, Honavar J, Brandon AP, Evans CA, Muthalaly R, et al. Estrogen alleviates sex-dependent differences in lung bacterial clearance and mortality secondary to bacterial pneumonia after traumatic brain injury. *J Neurotrauma* 2021;38:989–99.
- Röhrig C, Huemer M, Lorgé D, Luterbacher S, Phothaworn P, Schefer C, et al. Targeting hidden pathogens: cell-penetrating enzybiotics eradicate intracellular drug-resistant *Staphylococcus aureus*. *mBio* 2020;11:e00209–20.
- Scalise A, Bianchi A, Tartaglione C, Bolletta E, Pierangeli M, Torresetti M, et al. Microenvironment and microbiology of skin wounds: the role of bacterial biofilms and related factors. *Semin Vasc Surg* 2015;28:151–9.
- Schwartz DJ, Langdon AE, Dantas G. Understanding the impact of antibiotic perturbation on the human microbiome [published correction appears in *Genome Med* 2021;13:26. *Genome Med* 2020;12:82.
- Smythe P, Wilkinson HN. The Skin microbiome: current landscape and future opportunities. *Int J Mol Sci* 2023;24:3950.
- Stojadinovic O, Yin N, Lehmann J, Pastar I, Kirsner RS, Tomic-Canic M. Increased number of Langerhans cells in the epidermis of diabetic foot ulcers correlates with healing outcome. *Immunol Res* 2013;57:222–8.
- Summerfield A, Meurens F, Ricklin ME. The immunology of the porcine skin and its value as a model for human skin. *Mol Immunol* 2015;66:14–21.
- Tacconelli E, De Angelis G, Cataldo MA, Pozzi E, Cauda R. Does antibiotic exposure increase the risk of methicillin-resistant *Staphylococcus aureus* (MRSA) isolation? A systematic review and meta-analysis. *J Antimicrob Chemother* 2008;61:26–38.
- Tedersoo L, Albersen M, Anslan S, Callahan B. Perspectives and benefits of high-throughput long-read sequencing in microbial ecology. *Appl Environ Microbiol* 2021;87:e0062621.
- Trübe P, Hertlein T, Mrochen DM, Schulz D, Jorde I, Krause B, et al. Bringing together what belongs together: optimizing murine infection models by using mouse-adapted *Staphylococcus aureus* strains. *Int J Med Microbiol* 2019;309:26–38.
- Verbanic S, Shen Y, Lee J, Deacon JM, Chen IA. Microbial predictors of healing and short-term effect of debridement on the microbiome of chronic wounds. *NPJ Biofilms Microbiomes* 2020;6:21.
- Wasko R, Bridges K, Pannone R, Sidhu I, Xing Y, Naik S, et al. Langerhans cells are essential components of the angiogenic niche during murine skin repair. *Dev Cell* 2022;57:2699–713.e5.
- Wilkinson HN, Hardman MJ. Wound healing: cellular mechanisms and pathological outcomes. *Open Biol* 2020;10:200223.
- Wilkinson HN, Iveson S, Catherall P, Hardman MJ. A novel silver bioactive glass elicits antimicrobial efficacy against *Pseudomonas aeruginosa* and *Staphylococcus aureus* in an ex vivo skin wound biofilm model. *Front Microbiol* 2018;9:1450.
- Wilkinson HN, Kidd AS, Roberts ER, Hardman MJ. Human ex vivo wound model and whole-mount staining approach to accurately evaluate skin repair. *J Vis Exp* 2021:168.
- Williams H, Campbell L, Crompton RA, Singh G, McHugh BJ, Davidson DJ, et al. Microbial host interactions and impaired wound healing in mice and humans: defining a role for BD14 and NOD2. *J Invest Dermatol* 2018;138:2264–74.
- Zhang M, Jiang Z, Li D, Jiang D, Wu Y, Ren H, et al. Oral antibiotic treatment induces skin microbiota dysbiosis and influences wound healing. *Microb Ecol* 2015;69:415–21.
- Zhang XZ, Wu CY, Wu ZW, Xu LX, Jiang FT, Chen HW. Association between the diabetic foot ulcer and the bacterial colony of the skin based on 16s rRNA sequencing: an observational study. *Clin Cosmet Investig Dermatol* 2023;16:2801–12.
- Zipperer A, Konnerth MC, Laux C, Berscheid A, Janek D, Weidenmaier C, et al. Human commensals producing a novel antibiotic impair pathogen colonization [published correction appears in *Nature* 2016;539:314]. *Nature* 2016;535:511–6.



This work is licensed under a Creative Commons Attribution 4.0 International License. To view a copy of this license, visit <http://creativecommons.org/licenses/by/4.0/>

SUPPLEMENTARY MATERIALS AND METHODS

Biofilm testing

Bacteria were subcultured to an optical density of 0.4 at 600 nm and adjusted to between 5×10^5 and 1×10^6 colony-forming units/ml before seeding onto 0.2 μm polycarbonate membranes. Bacteria were treated with XZ.700 (100 $\mu\text{g}/\text{ml}$) or vehicle (0.01% Tween 20 in distilled water) 2 hours after seeding and collected for enumeration or live/dead staining 16 hours after seeding. Biofilms were enumerated by vortexing in 5 ml borosilicate glass beads and 1 ml citrate buffer (pH 4.5) to neutralize XZ.700. Resuspended biofilm bacteria were serially diluted in Mueller Hinton broth and plated on Mueller Hinton agar (Oxoid, Hampshire, United Kingdom).

Live/dead staining

The LIVE/DEAD BacLight Bacterial Viability Kit (Thermo Fisher Scientific) was used to visualize methicillin-resistant *Staphylococcus aureus* biofilm viability after XZ.700 treatment. Biofilms were stained as per the manufacturer's instructions and visualized on an LSM 710 confocal laser scanning microscope (Carl Zeiss, Oberkochen, Germany) equipped with 488-nm argon and 561-nm and 633-nm diode-pumped solid-state lasers. Pinhole size was equalized among lasers for optimum confocality. Representative z-stacks were captured at $\times 20$ magnification. Biofilm thickness was measured in ImageJ (National Institute of Health, Bethesda, MD).

Biofilm coculture

Coculture biofilms of *S aureus* and *S epidermidis* were prepared to confirm the selectivity and efficacy of XZ.700 against *S aureus*. Biofilm suspensions were prepared, and bacteria were seeded onto nitrocellulose membranes at 90% *S epidermidis* to 10% methicillin-resistant *S aureus*. Bacteria were treated, and biofilms were collected as mentioned earlier. For enumeration, antibiotic-selective agar was prepared (on the basis of Vitek 2 profiling data and confirmation of antibiotic breakpoints). Methicillin-resistant *S aureus* was enumerated on Mueller Hinton agar containing fusidic acid (50 $\mu\text{g}/\text{ml}$), whereas *S epidermidis* was enumerated on Mueller Hinton agar containing trimethoprim (1 $\mu\text{g}/\text{ml}$).

Microbiome sequencing analysis

DNA sequences were processed through a custom-built bioinformatics pipeline using VIPER High-Performance Computing hardware (University of Hull, Hull, United Kingdom). Briefly, data were base called using Guppy (version 4.4.2), demultiplexed using Qcat (version 1.1.0), and then filtered to remove any human or low complexity reads (Minimap2, version 2.15; Samtools, version 1.3.1; Prinseq-lite, version 0.20.4). Sequences were classified using Centrifuge (version 1.0.4), and contaminating reads were removed using microDecon (version 1.0.2). A total of 9,097,507 read counts were generated, encompassing 9441 operational taxonomic units (OTUs), spanning 3 domains (bacteria, eukaryotes, and archaea) plus viruses. Of the 9441 OTUs identified, 1847 OTUs appeared once only and were therefore removed. Across the samples, the average read count was 189,531 (minimum = 10,825; maximum = 662,080). Alpha diversity was assessed by richness (Chao) and diversity (Simpson), whereas beta diversity was shown

through principal coordinate analysis of Bray–Curtis distances using MicrobiomeAnalyst (Chong et al, 2020). Relative abundance was determined from OTUs and visualized using R package ggplot2. Hierarchical clustering of the top 150 most variable OTUs was performed on reads that were normalized through variance-stabilized transformation in R package DESeq2 (Love et al, 2014). Data were clustered using Euclidian distance and Ward D2's method within the R package gplots (Warnes et al, 2020).

Animal experimentation

Three female Gottingen Minipigs (aged ~ 6 months and weighing ~ 16 kg) were obtained from Ellegaard Minipigs and housed at the University of Leeds under a 12-hour light:dark cycle with once daily feeding and water provided ad libitum. Animal procedures were carried out under full United Kingdom Home Office regulations (project license P81E9540D). Animals were fasted for 12 hours before general anesthesia. Pigs were sedated using a mixture of Stresnil (Azaperone) (2 mg/kg, intramuscular) and Hypnovel (Midazolam) (0.3 mg/kg, intramuscular), and then general anesthesia was induced and maintained using isoflurane and oxygen. Buprenorphine (0.01 mg/kg, intramuscular) was administered immediately after surgery and at each dressing change. The pigs recovered under warmed conditions after each anesthetic episode.

On day 0, the flank skin of the pigs was clipped, and prospective wound sites were swabbed for bacterial enumeration and metagenomic profiling. The skin was then washed using an aseptic cleanser (5% chlorhexidine), shaved, and cleaned with 70% ethanol. Full-thickness excisional wounds (12-mm diameter) were created using biopsy punches. Wounds were treated with XZ.700 (1000 $\mu\text{g}/\text{ml}$) or vehicle buffer at contralateral sites. Wounds were covered with a film dressing (V.A.C. VIA drape, 3M, Saint Paul, MN), and a purpose-made Gottingen Minipig jacket (Lomir Biomedical, Québec, Canada) was used to protect the overlying dressings from damage (as described in Brownhill et al [2021]). On postwounding days 4, 8, 12, and 16, animals were reanesthetized, with periwound and wound regions swabbed for bacterial enumeration and metagenomic profiling before applying fresh treatments and dressings.

Tissue collection

Animals were culled using a UK Home Office Schedule 1 compliant method (intravenous pentobarbital sodium 20% w/v) on day 16 after wounding. Final swabs were collected, and wounds were harvested for histological analysis (in 10% buffered formal saline).

Bacterial enumeration from porcine swabs

For *S aureus*-specific colony-forming unit counts, skin and wound regions were swabbed with a PBS-saturated cotton tip and placed in an Eppendorf tube containing XZ.700-neutralizing buffer. Cotton tips were vortexed and centrifuged to collect supernatant, which was then serially diluted in Mueller Hinton broth and plated on CHROMagar Staph aureus (Chromagar, Paris, France). Counts are reported as \log_{10} -transformed colony-forming units/cm² of swabbed area.

Metagenomic sequencing from porcine skin/wound swabs

Microbial DNA was extracted from FLOQ swabs, sequenced, and processed as described earlier.

Histological analysis

Tissue was stained with Shandon's Haematoxylin (Eprelia, Runcorn, United Kingdom) and Eosin B (Merck, Darmstadt, Germany) to measure wound area and granulation tissue depth. Picrosirius red staining enabled the assessment of granulation tissue maturity (Wilkinson et al, 2019). Immunofluorescent staining was achieved using rabbit anti-*Iba1* (EPR16588; Abcam, Cambridge, United Kingdom), mouse anti-*Arg1* (E-2; Santa Cruz Biotechnology, Dallas, TX), mouse anti- α -smooth muscle actin (1A4; Abcam) and mouse anti-langerin (Leica Biosystems, Wetzlar, Germany). Primary antibodies were detected using Alexa Fluor-conjugated secondary antibodies (Thermo Fisher Scientific), and slides were mounted with Mowiol 488 containing 1,4-diazabicyclo[2.2.2]octane (both from Merck) and DAPI (Thermo Fisher Scientific). Brightfield images were acquired on a Nikon E400 (Tokyo, Japan) with SPOT camera (SPOT Imaging, Sterling Heights, MI). Fluorescent images were captured using an LSM 710 confocal microscope. Wound measurements, positive cell numbers, and staining intensity were determined using ImageJ.

RNA sequencing

RNA was extracted from human ex vivo wounds by homogenizing in TRIzol and purifying using the PureLink RNA Mini Kit. RNA sequencing was performed using an Illumina platform with paired-end method (error rate < 0.04%). HISAT2 was used to align the sequenced library to the reference genome, and differential expression analysis was performed on RNA-sequencing count data using DESeq2 with a cutoff of $P < .05$ and fold change = 1.5 (service provided by Novogene, Cambridge, United Kingdom). Hierarchical clustering was performed on the top 250 most variable differentially expressed genes (described for microbiome data), with functional annotation performed in the DAVID (Database for Annotation, Visualization and Integrated Discovery) (highlighting the key

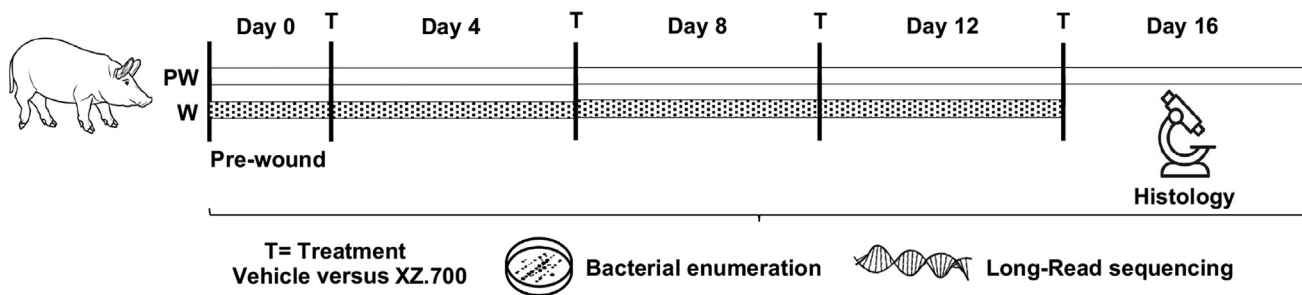
biological process for each cluster). The volcano plot of differentially expressed genes was created using the R package EnhancedVolcano. Enrichment analysis was performed on differentially expressed genes using the ShinyGO web package (Ge et al, 2020).

Supernatant preparation

Bacterial colonies were isolated from porcine skin using CHROMagar Staph aureus, and identity was confirmed using long-read sequencing. Supernatants of secreted bacterial products were prepared from overnight cultures by pelleting cells and sterile filtering the acellular liquid fraction. Supernatants were then added topically to human ex vivo skin wounds cultured at the air-liquid interface for 2 days at 35 °C and 5% carbon dioxide. Biopsies were collected in neutral buffered formalin solution, and wholemount staining was performed to assess wound closure rates (as detailed in Wilkinson et al [2021]).

SUPPLEMENTARY REFERENCES

- Brownhill VR, Huddleston E, Bell A, Hart J, Webster I, Hardman MJ, et al. Pre-clinical assessment of single-use negative pressure wound therapy during in vivo porcine wound healing. *Adv Wound Care (New Rochelle)* 2021;10:345–56.
- Chong J, Liu P, Zhou G, Xia J. Using MicrobiomeAnalyst for comprehensive statistical, functional, and meta-analysis of microbiome data. *Nat Protoc* 2020;15:799–821.
- Ge SX, Jung D, Yao R. ShinyGO: a graphical gene-set enrichment tool for animals and plants. *Bioinformatics* 2020;36:2628–9.
- Love MI, Huber W, Anders S. Moderated estimation of fold change and dispersion for RNA-seq data with DESeq2. *Genome Biol* 2014;15:550.
- Warnes GR, Bolker B, Bonebakker L, Gentleman R, Huber W, Liaw A, et al. Package gplots: various R programming tools for plotting data. <https://CRAN.R-project.org/package=gplots>; 2020. (accessed June 7, 2023).
- Wilkinson HN, Kidd AS, Roberts ER, Hardman MJ. Human ex vivo wound model and whole-mount staining approach to accurately evaluate skin repair. *J Vis Exp* 2021:168.
- Wilkinson HN, Upson SE, Banyard KL, Knight R, Mace KA, Hardman MJ. Reduced iron in diabetic wounds: an oxidative stress-dependent role for STEAP3 in extracellular matrix deposition and remodeling. *J Invest Dermatol* 2019;139:2368–77.e7.



Supplementary Figure S1. Experimental setup for porcine microbiome modulation study. Swabs for bacterial enumeration and long-read sequencing were taken at baseline and from PW and W regions at each assessed time point after injury. Endolysin was applied fresh (after swabbing) at days 0, 4, 8, and 12 after injury. Wounds were collected on day 16 for histological analysis. n = 3 pigs per group. PW, periwound; W, wound.